Journal of Biomedical Optics

SPIEDigitalLibrary.org/jbo

Method for rapid multidiameter single-fiber reflectance and fluorescence spectroscopy through a fiber bundle

Christopher L. Hoy
Ute A. Gamm
Henricus J. C. M. Sterenborg
Dominic J. Robinson
Arjen Amelink

SPIE

Method for rapid multidiameter single-fiber reflectance and fluorescence spectroscopy through a fiber bundle

Christopher L. Hoy, Ute A. Gamm, Henricus J. C. M. Sterenborg, Dominic J. Robinson, and Arjen Amelink
Erasmus Medical Center, Center for Optical Diagnostics and Therapy, Department of Radiation Oncology,
P.O. Box 2040, 3000 CA Rotterdam, The Netherlands

Abstract. We have recently demonstrated a means for quantifying the absorption and scattering properties of biological tissue through multidiameter single-fiber reflectance (MDSFR) spectroscopy. These measurements can be used to correct single-fiber fluorescence (SFF) spectra for the influence of optical properties, enabling quantification of intrinsic fluorescence. In our previous work, we have used a series of pinholes to show that selective illumination and light collection using a coherent fiber bundle can simulate a single solid-core optical fiber with variable diameter for the purposes of MDSFR spectroscopy. Here, we describe the construction and validation of a clinical MDSFR/SFF spectroscopy system that avoids the limitations encountered with pinholes and free-space optics. During one measurement, the new system acquires reflectance spectra at the effective diameters of 200, 600, and 1000 μm, and a fluorescence spectrum at an effective diameter of 1000 μm. From these spectra, we measure the absolute absorption coefficient, $\boldsymbol{\mu}_a$, reduced scattering coefficient, $\boldsymbol{\mu}_s'$, phase function parameter, $\boldsymbol{\gamma}$, and intrinsic fluorescence, $\boldsymbol{Q}\mu_{a,x}^f$, across the measured spectrum. We validate the system using Intralipid- and polystyrene sphere-based scattering phantoms, with and without the addition of the absorber Evans Blue. Finally, we demonstrate the combined MDSFR/SFF of phantoms with varying concentrations of Intralipid and fluorescein, wherein the scattering properties are measured by MDSFR and used to correct the SFF spectrum for accurate quantification of $\boldsymbol{Q}\mu_{a,x}^f$. *© 2013 Society of Photo-Optical Instrumentation Engineers (SPIE)* [DOI: 10.1117/1.JBO.18.10.107005]

Keywords: fluorescence spectroscopy; reflectance spectroscopy; scattering; tissue optics; optical property measurement.

Paper 130447R received Jul. 3, 2013; revised manuscript received Aug. 21, 2013; accepted for publication Aug. 23, 2013; published online Oct. 14, 2013.

1 Introduction

Optical spectroscopy of tissue is a powerful technique that provides a variety of diagnostically useful information about tissue optical properties and constituents.[1,2] Reflectance spectroscopy contains information about the presence and concentration of tissue chromophores as well as ultrastructural information related to scattering.[2] Meanwhile, fluorescence spectroscopy has the ability to detect endogenous molecules such as NADH and collagen as well as exogenous fluorescent markers or drugs.[3] Optical spectra acquired from tissue contain the competing effects of all tissue optical properties and are also highly dependent on illumination and detection geometry. As a result, the isolation and quantitative measurement of individual tissue optical properties and tissue constituents present a major challenge in optical spectroscopy.

Single-fiber reflectance (SFR) spectroscopy, in which the illumination and detection are performed by the same optical fiber, can be used to address this challenge.In this geometry, the measurement volume is confined to shallow depths, which, while dependent on the optical properties, are on the order of the fiber diameter.[4,5]Additionally, the measurement is sensitive to the scattering phase function.[6] As such, SFR spectroscopy may be well suited for detection of localized changes to the tissue microstructure that are expected to accompany early onset of disease. Additionally, the compact and simple probe design allows easy incorporation of small-diameter SFR probes into many clinical tools, such as endoscopic catheters[7,8] and FNA needles.[9,10]

Recently, our group has shown that the tissue absorption coefficient, $\boldsymbol{\mu}_a$ [mm^{-1}] (in this article, all wavelength-dependent variables are presented in boldface), can be accurately quantified without prior knowledge of the tissue scattering properties from an SFR measurement through the use of empirical models for the average photon path length and the collected SFR in the absence of absorption.[11] Decomposition of $\boldsymbol{\mu}_a$ into the constituent absorption spectra of known tissue chromophores enables accurate measurement of chromophore concentrations and microvascular parameters such as local blood oxygen saturation, blood volume fraction, and mean vessel diameter, which can be used for differentiating between healthy and cancerous tissue.[10] Due to the sensitivity of the SFR geometry to the scattering phase function, we have shown that acquiring at least two successive SFR measurements with different fiber diameters enables quantification of the reduced scattering coefficient, $\boldsymbol{\mu}_s' = (1-\boldsymbol{g}_1)\boldsymbol{\mu}_s$ [mm^{-1}], and the phase function parameter $\boldsymbol{\gamma} = (1-\boldsymbol{g}_2)/(1-\boldsymbol{g}_1)$[-] as well.[12,13] These scattering parameters are functions of the first- and second-Legendre moments of the scattering phase function, $\boldsymbol{g}_1$[-] and $\boldsymbol{g}_2$[-], where $\boldsymbol{\gamma}$ represents the likelihood of large-angle backscattering events. Specifically, an increase in $\boldsymbol{\gamma}$ indicates a decrease in large-angle backscattering. The scattering phase function is directly related to the tissue refractive index correlation function through a Fourier transform relationship;[14,15] thus, quantitative measurement of $\boldsymbol{\mu}_s'$ and $\boldsymbol{\gamma}$ can provide insight into the tissue microstructure, which is useful in diagnosing early onset of disease. The MDSFR spectroscopy

Address all correspondence to: Christopher L. Hoy, Erasmus Medical Center, Center for Optical Diagnostics and Therapy, Department of Radiation Oncology, P.O. Box 2040, 3000 CA Rotterdam, The Netherlands. Tel: +31-107032134; Fax: +31-107032141; E-mail: c.1hoy@erasmusmc.nl

0091-3286/2013/$25.00 © 2013 SPIE

technique has been validated in both Monte Carlo simulations[12,16] and tissue-mimicking liquid optical phantoms,[13] and has recently been used *in vivo* to quantify optical properties in a murine cancer model.[17]

The tissue optical properties measured with the multidiameter single-fiber reflectance (MDSFR) technique can be used for correction of fluorescence spectroscopy, where *in situ* quantification of fluorophore concentrations from the fluorescence spectra is complicated by the effects of tissue optical properties on the excitation and emission of light. We have recently developed a semi-empirical model for single-fiber fluorescence (SFF) spectroscopy that corrects for the effects of tissue optical properties at both the excitation and emission wavelengths to enable accurate quantification of intrinsic fluorescence,[18] given as the product of the tissue fluorophore absorption coefficient at the excitation wavelength, $\mu_{a,x}^{f}$ [mm^{-1}], and the quantum efficiency across the emission spectrum, $\boldsymbol{Q}$[-]. Section 2.1 provides further details regarding the MDSFR and SFF models and their use.

Conducting MDSFR spectroscopy by sequential placement of multiple optical fibers is time consuming and sensitive to errors in probe placement, making this approach clinically impractical. We have previously demonstrated a means of simulating a single fiber with a variable diameter using a coherent fiber bundle and a series of pinholes to control the effective fiber diameter.[19] While successful, this technique is still time consuming and limited by back reflections.

Here, we present the development and characterization of an MDSFR/SFF system which uses a 19-core fiber bundle and eliminates free-space optical components for improved robustness, signal-to-noise ratio (SNR), and acquisition time. In this article, we summarize the MDSFR and SFF models, the critical aspects of the system design, calibration and measurement algorithms, and the characterization and validation of the system using liquid optical phantoms.

2 Methods and Materials

2.1 *MDSFR and SFF Models for the Extraction of Optical Properties*

Recently, our group has developed semi-empirical models for the collected SFR in the absence of absorption, $\boldsymbol{R}_{SF}^{0}$ [%],[16] and the effective photon path length for SFR, $\langle \boldsymbol{L}_{SFR} \rangle$ [mm],[4,5] based on experimentally validated Monte Carlo simulations. From a single SFR measurement, the tissue absorption coefficient, $\boldsymbol{\mu}_a$, can be determined using a modified Beer–Lambert law relationship

$$\boldsymbol{R}_{SF} = \boldsymbol{R}_{SF}^{0} e^{-\boldsymbol{\mu}_a \langle \boldsymbol{L}_{SFR} \rangle}, \tag{1}$$

with the model for effective SFR path length

$$\frac{\langle \boldsymbol{L}_{SFR} \rangle}{d_f} = \frac{C_{PF} p_1}{(\boldsymbol{\mu}_s' d_f)^{p_2} [p_3 + (\boldsymbol{\mu}_a d_f)^{p_3}]}, \tag{2}$$

and using the model for $\boldsymbol{R}_{SF}^{0}$,

$$\boldsymbol{R}_{SF}^{0} = \eta_{lim}(1 + p_6 e^{-p_4 \boldsymbol{\mu}_s' d_f}) \left[\frac{(\boldsymbol{\mu}_s' d_f)^{p_5}}{p_4 + (\boldsymbol{\mu}_s' d_f)^{p_5}} \right], \tag{3}$$

with a background scattering model.[11,17] In the above equations, η_{lim} is the collection efficiency at the diffusion limit, given as 2.7% for a fiber numerical aperture of 0.22 in a medium of refractive index 1.38.[20] The parameters $[C_{PF}, p_1, p_2, p_3]$ and $[p_4, p_5, p_6]$ are fitted parameters. The fitted parameters have been previously determined by Monte Carlo simulations of the SFR covering the parameter ranges of $d_f = [0.2-1.0]$ mm, $\mu_s' = [0.3-3.6]$ mm^{-1}, and $\mu_a = [0-3.0]$ mm^{-1} using a modified and unmodified Henyey–Greenstein phase functions with $g_1 = [0.8, 0.9, 0.95]$ and $\gamma = [1.4-1.9]$.[4,6,11] For $[C_{PF}, p_1, p_2, p_3]$ and $[p_4, p_5, p_6]$, the values [0.944, 1.54, 0.18, 0.64] and [6.82, 0.969, 1.55], respectively, were found to minimize the residual error between the SFR model and the simulations.[4,6,11]

Due to the overlapping source and detector geometry of the single-fiber measurement, the measured reflectance spectra are sensitive to the scattering phase function. Specifically, changes in phase function result in a linear shift of $\langle \boldsymbol{L}_{SFR} \rangle$ given by the constant C_{PF}. In $\boldsymbol{R}_{SF}^{0}$, the fitted parameters $[p_4, p_5, p_6]$ are phase function dependent. In analyzing a single SFR measurement, the error in estimating $\boldsymbol{\mu}_s'$ that arises from not knowing the correct phase function parameters $[p_4, p_5, p_6]$ is balanced by the offsetting error arising from the assumption of C_{PF}, which allows accurate quantification of $\boldsymbol{\mu}_a$ to within an RMS residual of 7.5% without accurate knowledge of scattering or phase function properties.[11]

Recently, we have demonstrated that $[p_4, p_5, p_6]$ are specifically sensitive to the phase function parameter, $\boldsymbol{\gamma}$, where $[p_4, p_5, p_6] = [2.31\boldsymbol{\gamma}^2, 0.57\boldsymbol{\gamma}, 0.631\boldsymbol{\gamma}^2]$.[16] As a result, successive SFR measurements with at least two fiber diameters enable simultaneous solution of Eq. (3) for absolute quantification of $\boldsymbol{\mu}_s'$ and $\boldsymbol{\gamma}$ over the measured wavelength range.[12,13]

Similar to the SFR model, we have created a semi-empirical model of SFF to correct for the effects of tissue scattering and absorption on the fluorescence excitation and emission photons. In this model, the ratio of collected emission photons to excitation photons, $\boldsymbol{F}_{SF}$[−], is corrected for tissue absorption properties using a modified Beer–Lambert law relationship

$$\boldsymbol{F}_{SF} = \boldsymbol{F}_{SF}^{0} e^{-\bar{\boldsymbol{\mu}}_a \langle \boldsymbol{L}_{SFF} \rangle}, \tag{4}$$

where $\bar{\boldsymbol{\mu}}_a$ is the average of the absorption coefficient at the excitation and emission wavelengths and $\langle \boldsymbol{L}_{SFF} \rangle$ is the average effective path length for SFF, given by[18,21]

$$\frac{\langle \boldsymbol{L}_{SFF} \rangle}{d_f} = 0.71(\bar{\boldsymbol{\mu}}_s' d_f)^{-0.36} \frac{1 + 1.81\sqrt{\bar{\boldsymbol{\mu}}_s' d_f}}{1 + (\boldsymbol{\mu}_a d_f)}. \tag{5}$$

Here, $\bar{\boldsymbol{\mu}}_s'$ is the average of the reduced scattering coefficient at the excitation and emission wavelengths. The absorption-corrected fluorescence ratio, $\boldsymbol{F}_{SF}^{0}$, is then corrected for tissue scattering in a second step, which enables calculation of the wavelength-dependent intrinsic fluorescence

$$\boldsymbol{Q}\mu_{a,x}^{f} = \frac{\boldsymbol{F}_{SF}^{0}}{d_f \upsilon_n \boldsymbol{S}}, \tag{6}$$

where υ_n is a fiber diameter dependent correction factor,[18] and correction for scattering is given by the dimensionless function

$$\boldsymbol{S} = 0.0935(\bar{\boldsymbol{\mu}}_s' d_f)^{-0.31} e^{\left(\frac{-1}{0.31(\mu_{s,x}' d_f)+1} - \frac{1.61}{0.31(\boldsymbol{\mu}_{s,m}' d_f)+1} \right)}. \tag{7}$$

Here, $\mu_{s,x}'$ and $\boldsymbol{\mu}_{s,m}'$ are the reduced scattering coefficients at the excitation and emission wavelengths, respectively. Integrating

Eq. (6) over the emission bandwidth of a fluorophore yields the total intrinsic fluorescence, $\boldsymbol{Q}\mu_{a,x}^{f}$, of the fluorophore at the excitation wavelength. Thus, combining MDSFR and SFF spectroscopy techniques enables absolute quantitative measurement of $\boldsymbol{\mu}_a$, $\boldsymbol{\mu}_s'$, $\boldsymbol{\gamma}$, and $\boldsymbol{Q}\mu_{a,x}^{f}$ within a localized volume of tissue.

2.2 *Design of the MDSFR/SFF System*

The MDSFR/SFF system is based upon a custom-built fiber bundle that consists of 19 optical fibers with core sizes of 200 μm (CeramOptec, Germany). At the distal end, the fibers are bundled into three concentric groups comprised of one, six, and 12 fibers, as shown in Fig. 1. Using a CCD camera, the outer diameter of the middle and outer rings of fiber cores were found to be 650 and 1060 μm, respectively. At the opposite end, the fibers are individually terminated to allow direct fiber optic coupling to individual cores, as seen in Fig. 1(c). Each fiber in the bundle is trifurcated to be connected to (1) a fiber delivering light from a halogen lamp (HL-2000-FHSA, Ocean Optics, The Netherlands), (2) a fiber delivering light from a 365-nm LED (NC4U133A, Nichia, Japan) or a 780-nm LED (L780-06-55, Marubeni, USA), and (3) a fiber collecting light returning from the sample and delivering it to one of the three spectrometers. A series of fiber optic interconnects, along with three computer-controlled shutters, enables illumination and spectroscopic detection of the center fiber, the middle ring, and the outer ring of fibers, independently. The optical pathways are shown schematically in Figs. 1(c) and 1(d). Homogeneous illumination of each fiber in the bundle was verified to be within a standard deviation of 7.6% using a CCD camera.

For detection, spectra are acquired from the three groups of fibers using three spectrometers (two S2000s, one USB2000+, Ocean Optics, The Netherlands) with an overlapping spectral range of 350 to 1000 nm. Each spectrometer is filtered by a long-pass filter with a 385 nm cut-off wavelength (GL-GG385-12, Avantes, The Netherlands) to remove fluorescence excitation light. For SFF, all fibers in the bundle are illuminated simultaneously by the 365-nm LED while detecting on all spectrometers, thus providing an SFF measurement using the largest effective fiber diameter of 1.0 mm.

Lastly, a laptop running LabView coordinates fiber illumination, merging of the three spectrometer channels, calibration, and display of calibrated MDSFR and SFF spectra. A foot pedal is used to initiate each combined MDSFR/SFF measurement, which requires <8 s to complete in the current configuration.

2.3 *System Calibration*

Accurate quantification of tissue fluorescence and optical properties requires careful calibration to account for the spectral illumination, transmission, and detection efficiencies of the measurement system. The calibration of the MDSFR/SFF system consists of three steps: integrating sphere calibration,[13] reference optical phantom calibration, and calibrated lamp calibration. Each step requires less than a minute to complete and calibration need only be conducted once per day.

2.3.1 *Integrating sphere calibration*

The MDSFR/SFF system merges spectra from different spectrometers to create measurements with varying effective fiber diameters. Correct merging of spectrometer channels first requires correction for differences in spectral sensitivity and transmission between channels, which can be achieved by comparing the spectra measured by each channel under uniform illumination. This is accomplished by inserting the probe into an integrating sphere, which is built into the MDSFR/SFF system, and illuminating the sphere with the halogen lamp through a side port. The spectra acquired from the center fiber ($\boldsymbol{I}_{center}^{int.sphere}$ [counts/s]) and middle ring of fibers ($\boldsymbol{I}_{middle}^{int.sphere}$) are then normalized by the spectrum acquired from the outer ring of fibers ($\boldsymbol{I}_{outer}^{int.sphere}$), taking into account the difference in signal levels due to the different number of fibers in each group. These spectra are used to arrive at wavelength-dependent weighting coefficients ($\boldsymbol{W}_{center}$[-] and $\boldsymbol{W}_{middle}$)for the two innermost channels:

$$\boldsymbol{W}_{center} = \frac{1}{12}\frac{\boldsymbol{I}_{outer}^{int.sphere}}{\boldsymbol{I}_{center}^{int.sphere}} \tag{8}$$

and

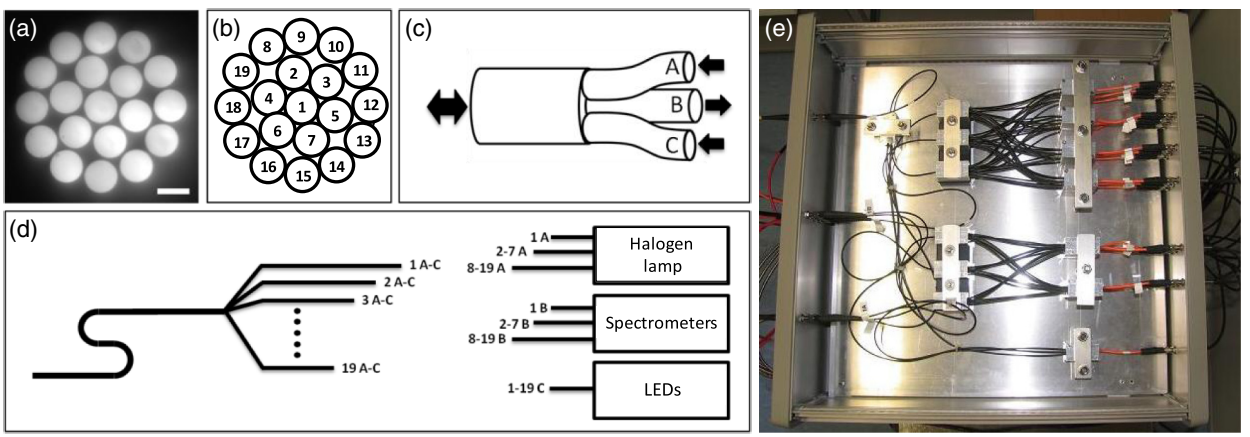

Fig. 1 The MDSFR/SFF system: (a) CCD image of the distal end of the fiber bundle probe showing the illumination uniformity between fiber cores. Scale bar is 200 μm. (b) Schematic representation of (a) with numbering of the fiber cores. (c) Detail schematic of the trifurcation at the proximal end of each fiber in the bundle. (d) Schematic of the fiber tree. (e) Photograph of the fiber tree used in the MDSFR/SFF system.

$$\boldsymbol{W}_{\text{middle}} = \frac{6}{12}\frac{\boldsymbol{I}_{\text{outer}}^{\text{int.sphere}}}{\boldsymbol{I}_{\text{middle}}^{\text{int.sphere}}}. \quad (9)$$

The weighting coefficients are calculated relative to the outer channel because this channel has the largest detection area and thus the largest SNR. During an MDSFR measurement, the spectra from each channel are combined using these weighting coefficients into effective single-fiber spectra with three different effective diameters, where

$$\boldsymbol{I}_{\text{small}}^{\text{eff}} = \boldsymbol{I}_{\text{center}}, \quad (10)$$

$$\boldsymbol{I}_{\text{med}}^{\text{eff}} = \boldsymbol{W}_{\text{center}}\boldsymbol{I}_{\text{center}} + \boldsymbol{W}_{\text{middle}}\boldsymbol{I}_{\text{middle}}, \quad (11)$$

and

$$\boldsymbol{I}_{\text{large}}^{\text{eff}} = \boldsymbol{W}_{\text{center}}\boldsymbol{I}_{\text{center}} + \boldsymbol{W}_{\text{middle}}\boldsymbol{I}_{\text{middle}} + \boldsymbol{I}_{\text{outer}}. \quad (12)$$

After illumination of the fiber bundle inside the integrating sphere, light from the 365-nm fluorescence excitation LED is guided through the bundle, followed by light from the 780-nm calibration LED. A photodetector mounted in the integrating sphere measures the output powers from each LED, which are required for SFF calibration.

2.3.2 *Reference optical phantom calibration*

After the individual spectral channels are combined into the effective single-fiber spectra, these spectra are then calibrated to account for the spectral illumination and transmission efficiencies and the spectrometer sensitivity for each effective fiber diameter. This calibration is achieved by acquiring MDSFR spectra from a water sample and from an Intralipid-based scattering optical phantom, which has been described in detail elsewhere.[19] The use of liquid calibration phantoms allows the probe to be submerged in the phantom during measurement and thus provides a more consistent measurement than achieved with highly reflective solid phantoms or reflectance standards, measurements of which are sensitive to probe contact conditions. The spectrum acquired from the water sample ($\boldsymbol{I}_{\text{water}}^{\text{eff}}$) originates from back reflections within the system and is subtracted from every measurement, while the spectra acquired from the Intralipid scattering phantom ($\boldsymbol{I}_{\text{cal}}^{\text{eff}}$) is compared with the absolute reflectance for this phantom ($\boldsymbol{R}_{\text{cal}}^{\text{sim}}$), which has been simulated for each effective fiber diameter using a Monte Carlo model. The resulting measurement is calibrated into absolute reflectance ($\boldsymbol{R}_{\text{SF}}$), where

$$\boldsymbol{R}_{\text{SF}} = \boldsymbol{R}_{\text{cal}}^{\text{sim}}\frac{\boldsymbol{I}_{\text{meas}}^{\text{eff}} - \boldsymbol{I}_{\text{water}}^{\text{eff}}}{\boldsymbol{I}_{\text{cal}}^{\text{eff}} - \boldsymbol{I}_{\text{water}}^{\text{eff}}}. \quad (13)$$

Equation (13) is used to calibrate the reflectance spectra from each effective fiber diameter independently, where the measured spectra, $\boldsymbol{I}^{\text{eff}}$, are given by Eqs. (10), (11), or (12), depending on the effective diameter.

In addition to MDSFR measurements of the phantoms with the halogen lamp, spectra are also acquired using the 780-nm LED for illumination through the 1000-μm nominal fiber diameter. The power from the 780-nm LED, $P_{780} = \int \boldsymbol{P}_{780}\mathrm{d}\lambda$, measured by the integrating sphere and the known reflectance of the Intralipid phantom at 780 nm enable calculation of the absolute system sensitivity at 780 nm, which is used to calibrate SFF measurements.

2.3.3 *Calibrated lamp calibration*

The final calibration step measures the spectral sensitivity of the system using a calibrated lamp with a known spectral irradiance (HL-2000-CAL, Ocean Optics, Duiven, The Netherlands). The fiber bundle probe is directly coupled to the light source, and the spectrum of the calibrated lamp, $\boldsymbol{I}_{\text{lamp}}^{\text{eff}}$, is acquired with the 1000-μm nominal fiber diameter. Using this measurement, the system sensitivity measured at 780 nm from the LED can be extended to cover the full wavelength range of the spectroscopy system. This allows calibration of the raw SFF spectra into units of spectral irradiance.

2.3.4 *Calibration of SFF spectra*

Use of the SFF model given in Eqs. (4)–(7) requires calibration of the measured SFF spectrum, $\boldsymbol{I}_{\text{SFF}}^{\text{eff}}$, into the ratio of emission photons to excitation photons at each emission wavelength, $\boldsymbol{F}_{\text{SF}}$.[18] Doing so requires knowledge of the combined transmission efficiency and sensitivity of the measurement system, $\boldsymbol{T}$ [counts/(s μW)], where

$$\boldsymbol{F}_{\text{SF}} = \frac{\boldsymbol{I}_{\text{SFF}}^{\text{eff}}\boldsymbol{T}^{-1}}{P_{\text{x}}(\lambda_{\text{x}}/\boldsymbol{\lambda}_{\text{m}})} \quad (14)$$

and P_{x} [μW] is the power of the excitation source measured at the fiber tip. The ratio of excitation to emission wavelengths, $\lambda_{\text{x}}/\boldsymbol{\lambda}_{\text{m}}$, is used to account for the difference in photon energies between the excitation source and the collected emission light. The wavelength dependent $\boldsymbol{T}$ can be calculated based on an absolute measure of transmission at a reference wavelength, provided here by the measured reflectance of the 780-nm LED in Intralipid

$$\int \boldsymbol{I}_{780}^{\text{eff}}\mathrm{d}\lambda = P_{780}\int \boldsymbol{T}\boldsymbol{R}_{\text{cal}}^{\text{sim}}\mathrm{d}\lambda, \quad (15)$$

and a relative measurement of spectral transmission across the entire wavelength range, provided by the calibrated lamp, where

$$\boldsymbol{I}_{\text{lamp}}^{\text{eff}} = \alpha\boldsymbol{P}_{\text{lamp}}^{\text{spec}}\boldsymbol{T}. \quad (16)$$

The parameter α [cm^2] is a wavelength-independent coupling factor that accounts for the fact that only a portion of the specified power from the calibrated lamp, $\boldsymbol{P}_{\text{lamp}}^{\text{spec}}$ [μW/cm^2], is coupled into the fiber bundle. The parameter α is based on the area and angular acceptance of the bundle and the separation distance between the lamp output and the fiber probe. As a result, Eqs. (15) and (16) represent two equations with two unknown parameters, where solution for α enables solving for the wavelength dependent $\boldsymbol{T}$ in Eq. (16).

2.4 *System Validation*

Because the fiber bundle used in this study is more coarse than the bundle used in our previous system (7 to 19 fibers used to represent a single solid-core fiber, instead of 1 k to 10 k),[19] and the effective SFR spectra are merged across multiple spectrometers, it is nonobvious whether or not the merged spectra acquired from the individual fibers are equivalent to the SFR spectra measured by a single solid-core fiber. To answer this

question, we have performed a series of experiments using liquid optical phantoms to confirm that the MDSFR and SFF spectra acquired with the system are both in agreement with our models for MDSFR and SFF and with the experimental MDSFR and SFF spectra acquired using single solid-core fibers of equal diameter.

First, a series of scattering and absorbing phantoms was measured by SFR using both the fiber bundle system and individual solid-core fibers with $d_f = [0.2, 0.6, 1.0]$ mm. The solid-core fiber diameters were chosen to closely match the diameters of the rings of fibers in the fiber bundle. The phantoms consisted of varying concentrations of Intralipid and the absorber Evans Blue in 0.9% NaCl solution to achieve $\mu_s'(611\text{ nm}) = [0.36, 0.53, 0.71, 1.1, 1.4, 1.8, 3.5, 5.3]$ mm^{-1} (Ref. 22) and $\mu_a(611\text{ nm}) = [0, 0.5, 1, 2, 3]$ mm^{-1}. To properly imitate a solid-core fiber for the purposes of SFR, the merged spectra from the MDSFR system must exhibit $\langle \boldsymbol{L}_{SFR} \rangle$ and $\boldsymbol{R}_{SF}$ equal to that of a solid-core fiber of a given diameter across the measured spectrum. In SFR spectroscopy, the path length has been found to have a fixed relationship with the mean sampling depth of the measurement,[4] and so demonstration of equivalent path length to single-fiber measurements demonstrates that the measurement depth is also equivalent. Path length equivalence was verified by measuring $\langle \boldsymbol{L}_{SFR} \rangle$ using Eq. (1) as in the previous studies,[5,19] where

$$\langle \boldsymbol{L}_{SFR} \rangle = -\frac{1}{\boldsymbol{\mu}_a} \ln\left(\frac{\boldsymbol{R}_{SF}}{\boldsymbol{R}_{SF}^0}\right). \tag{17}$$

The above relationship is dependent upon the ratio of the reflectance measurements; therefore, the calculation of effective path length does not require the assumption of a specific fiber diameter that is normally introduced during calibration [Eq. (13)]. For this analysis, Eq. (17) is evaluated at 611 nm, where the $\boldsymbol{\mu}_a$ of Evans Blue has its maximum. In addition to the path length, $\boldsymbol{R}_{SF}^0$ was compared between the MDSFR system and the solid-core fibers at $\lambda = [425,525,625,725,825]$ nm. For calibration of $\boldsymbol{R}_{SF}^0$ with the fiber bundle, simulated diameters of $d_f = [0.2, 0.6, 1.0]$ mm were used.

Next, MDSFR measurements were acquired from an optical phantom consisting of a fractal distribution of polystyrene spheres (Polybead Microspheres, Polysciences, Eppelheim, Germany) in 0.9% NaCl chosen to model a modified Henyey–Greenstein phase function, which has been described in Gamm et al.[13] The measurements were made with both the fiber bundle system and individual solid-core fibers for comparison of the extracted scattering parameters $\boldsymbol{\mu}_s'$ and $\boldsymbol{\gamma}$.

Finally, a series of phantoms was prepared with varying concentrations of Intralipid in phosphate buffered saline, both with and without 20 μM of fluorescein. The absorption coefficient of the fluorescein solution at 365-nm excitation, $\mu_{a,x}^f$, was measured with a spectrophotometer to be $7.6 \pm 0.1(10)^{-3}$ mm^{-1}. (In this article, all uncertainties are reported as 95% confidence intervals, unless otherwise specified.) MDSFR and SFF spectra were acquired from each phantom, where $\boldsymbol{\mu}_a$ and $\boldsymbol{\mu}_s'$ extracted from the MDSFR analysis were used to correct the SFF measurement and extract the intrinsic fluorescence $\boldsymbol{Q}\mu_{a,x}^f$.

3 Results

3.1 *Determination of Single-Fiber Equivalence and Effective Fiber Diameter*

Analyzing the effective photon path length in the Intralipid-based phantoms using Eq. (17), $\langle \boldsymbol{L}_{SFR} \rangle$ at 611 nm is observed to correlate well between the fiber bundle and the solid-core fibers with an overall Pearson correlation coefficient of $r = 0.987$ for the three effective diameters, as shown in Fig. 2(a). The RMS residual errors for the merged channels, $d_f = 1.0$ and 0.6 mm, are 3.93% and 5.93%, respectively. The measurements for $d_f = 0.2$ mm represent comparisons between two solid-core fibers because this channel consists of only one fiber core in the MDSFR system, and the increased scatter observed in some of these measurements arises from the reduction in signal from SFR measurements with decreasing dimensionless scattering coefficient, $\boldsymbol{\mu}_s' d_f$, as seen in Eq. (3).

The path-length analysis above relies only on the measured reflectance at one wavelength. To determine if the reconstructed spectra in the MDSFR system are equivalent to SFR spectra from solid-core fibers across the entire spectrum, the measured $\boldsymbol{R}_{SF}^0$ for both systems was compared. Figure 2(b) displays the correlation between the $\boldsymbol{R}_{SF}^0$ measured with the fiber bundle and the $\boldsymbol{R}_{SF}^0$ measured by the solid-core fiber for a range of wavelengths. The $\boldsymbol{R}_{SF}^0$ measurements are strongly correlated ($r = 1.000$) and RMS residual errors for the merged channels,

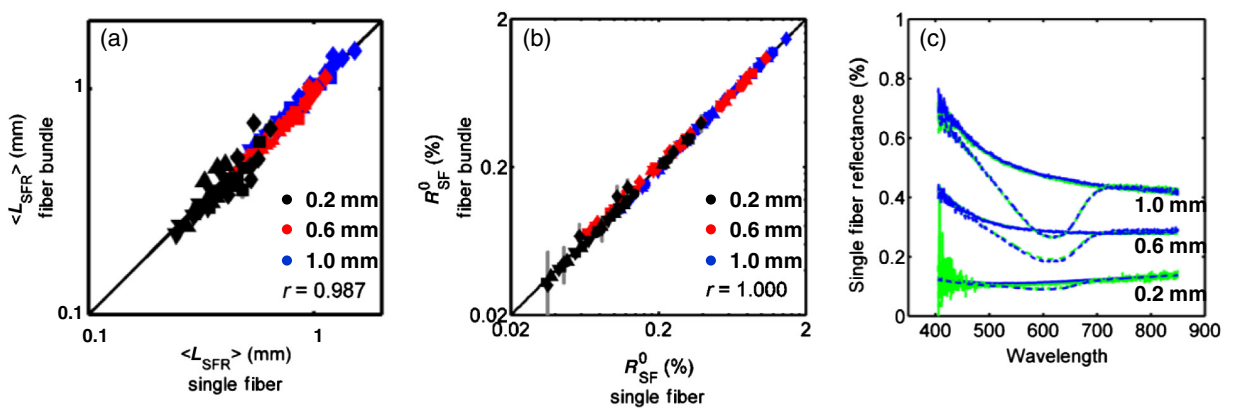

Fig. 2 Comparison of SFR measurements in Intralipid phantoms between the fiber bundle system and solid-core fibers. (a) Comparison of $\langle \boldsymbol{L}_{SFR} \rangle$ at 611 nm. Data correspond to $\mu_a(611\text{ nm})$ of 0.5 (diamond), 1 (square), 2 (upright triangle), and 3 (downward triangle) mm^{-1}, respectively. (b) Comparison of $\boldsymbol{R}_{SF}^0$ at 425 (diamond), 525 (square), 625 (upright triangle), 725 (downward triangle), and 825 (circle) nm, respectively. In (a) and (b), the blue, red, and black data correspond to fiber diameters of 1.0, 0.6, and 0.2 mm, respectively. (c) The plot of representative SFR spectra measured with the fiber bundle system (green) and solid-core fibers (blue) for $\mu_s'(611\text{ nm}) = 1.8$ mm^{-1}, $\mu_a(611\text{ nm}) = 0$ and 0.5 mm^{-1}.

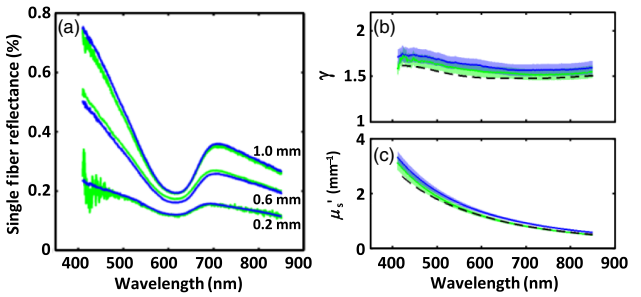

Fig. 3 Comparison of SFR measurements in Polybead phantoms between the fiber bundle system (green) and solid-core fibers (blue). (a) Plot of representative SFR spectra measured with the fiber bundle system and solid-core fibers. (b) Comparison of the extracted γ and (c) μ_s'. Dashed lines represent values predicted by Mie theory. Shaded bands in (b) and (c) represent the 95% confidence interval for each measurement.

$d_f = 1.0$ and 0.6 mm, are 3.06% and 3.83%, respectively. Figure 2(c) displays an overlay of representative SFR spectra measured by the fiber bundle and by the solid-core fibers.

3.2 *Validation of Extracted Optical Properties by MDSFR*

The MDSFR spectra acquired from the Polybead phantom using both the MDSFR/SFF system and individual solid-core fibers are shown in Fig. 3(a). As observed in the Intralipid phantoms, the reflectance spectra acquired from the Polybead phantoms using the MDSFR/SFF system are in good agreement with those of the 0.2-, 0.6-, and 1.0-mm diameter solid-core fibers. The extracted scattering properties of μ_s' and γ, shown in Fig. 3(b), also agree well with the solid-core fiber measurements, with overlapping 95% confidence intervals across the measured spectrum. In comparison with the scattering properties predicted by Mie theory, the predicted $\boldsymbol{\mu_s'}$ lies within the 95% confidence interval of the values extracted by the MDSFR/SFF system over the entire spectral range. The extracted $\boldsymbol{\gamma}$ is slightly higher than the $\boldsymbol{\gamma}$ predicted by theory, which has been attributed to the differences in higher-order moments between the modified Henyey–Greenstein phase function used to create the MDSFR model and the Mie phase function.[13,23]

Interestingly, the scattering properties measured by the MDSFR/SFF system are slightly closer to those predicted by Mie theory and our previous measurements[13] than the properties extracted from the solid-core fiber measurements presented here. This is likely due to the independent calibration and measurement of each solid-core fiber, which could allow small relative changes in the calibrated reflectance between fiber diameters. Because the calibration and measurement of each diameter in the MDSFR/SFF system occur in one step, the potential for differences in measurement condition between diameters is greatly reduced.

3.3 *Validation of SFF Through Extraction of* $\boldsymbol{Q\mu_{a,x}^f}$

The extraction of the intrinsic fluorescence of fluorescein in Intralipid scattering phantoms was used to validate quantitative fluorescence spectroscopy with the MDSFR/SFF device. In these measurements, the scattering properties of Intralipid-fluorescein phantoms were extracted from the MDSFR measurement and used to correct the SFF measurement for the effects of the optical properties. The intrinsic fluorescence $\boldsymbol{Q\mu_{a,x}^f}$ was then extracted by fitting the data to Eq. (6) by nonlinear regression. The resulting $\boldsymbol{Q\mu_{a,x}^f}$ was found to be $7.0 \pm 0.3(10)^{-3}$ mm^{-1}, which yields a $\boldsymbol{Q}$ of 0.92 ± 0.04 for the measured $\mu_{a,x}^f$ of $7.6 \pm 0.1(10)^{-3}$ mm^{-1}. The measured $\boldsymbol{Q}$ is in good agreement with the published value for fluorescein, $\boldsymbol{Q} = 0.88$, at the measured pH of 7.4.[24] Using the extracted $\boldsymbol{Q\mu_{a,x}^f}$ of $7.0(10)^{-3}$ mm^{-1}, the dimensionless SFF, $\boldsymbol{F_{SF}/d_f}$, was found to be in good agreement with Eq. (7) throughout the investigated range of dimensionless scattering coefficient, $\boldsymbol{\mu_s' d_f}$, as seen in Fig. 4.

4 Discussion

Based on the similarity observed in Figs. 2(c) and 3(a) between the SFR spectra measured by the fiber bundle system and solid-core fibers, we conclude that the merged spectra from the fiber bundle system do accurately represent spectra from single solid-core fibers across the entire measured spectral range. The consistency between the optical properties $\boldsymbol{\mu_a}$, $\boldsymbol{\mu_s'}$, $\boldsymbol{\gamma}$, and $\boldsymbol{Q\mu_{a,x}^f}$ measured by the fiber bundle system and the predicted values in both the Polybead and fluorescein phantoms further supports that the fiber bundle system accurately simulates single fibers with $d_f = [0.2, 0.6, 1.0]$ mm. Significantly, the scattering properties recovered from the fiber bundle system were found to be slightly closer to their predicted values than those recovered by separate single-fiber measurements, which illustrates the potential for small measurement errors when calibrating each fiber independently and demonstrates the sensitivity of the scattering property measurement to such errors.

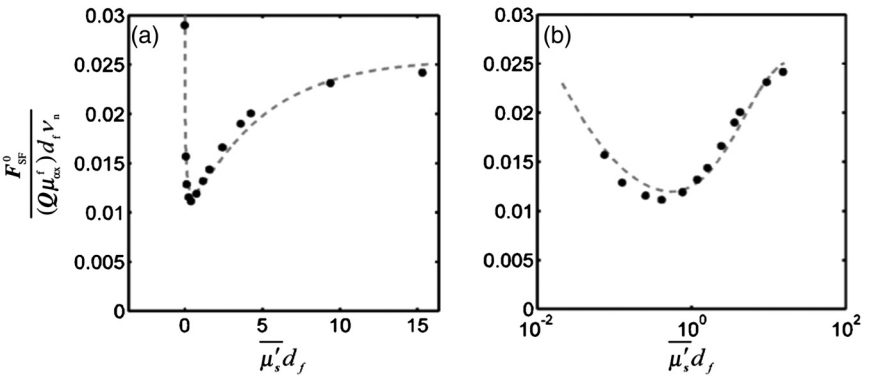

Fig. 4 The nondimensionalized SFF corresponding to the best fit of $\boldsymbol{Q\mu_{a,x}^f}$ to the data (black data points) and the predicted dependence on $\boldsymbol{\mu_s' d_f}$ (gray-dashed line) on (a) linear scale and (b) a semi-log scale.

As observed in our previous study,[13] the measured γ consistently over-predicted the true value for both the fiber bundle and single-fiber systems. This discrepancy has been predicted by simulations and attributed to subtle differences between the modeled modified Henyey–Greenstein phase function and the true Mie phase function. However, it is also important to note that the MDSFR technique relies upon accurate Monte Carlo simulation of Intralipid scattering and the use of Intralipid as a calibration reference. Therefore, the accuracy of the extracted optical properties depends on accurate knowledge of the Intralipid scattering coefficient and phase function. Additionally, the batch-to-batch variation of the Intralipid properties must be minimal. The optical properties of Intralipid have been extensively studied,[22] and observed batch-to-batch variations in scattering were found to be near 2% over a period of 7 years;[25] however, the sensitivity of our technique to Intralipid scattering could potentially play a role in the discrepancy between the measured and predicted γ in the Polybead phantoms.

The fiber bundle used in this study uses only a minimum number of fibers (7 or 19) to simulate a solid-core fiber, in contrast to our previous study in which each effective fiber diameter consists of thousands of small individual fibers. The successful simulation of solid-core fibers in both cases indicates that the coarseness of the fiber bundle has little impact on SFR measurements over the range of $\boldsymbol{\mu}_s' d_f$ investigated. This suggests that the use of a fiber bundle as a variable-diameter single fiber for MDSFR is broadly applicable to a range of fiber bundle geometries between these two extreme cases. As a result, alternative fiber bundle geometries can be considered to suit specific applications. For example, a probe with $d_f = [0.2, 0.4, 0.6]$ mm might be considered for an application wishing to focus on skin epithelial properties, while an alternative probe with $d_f = [0.8, 1.2, 1.5]$ mm could be employed to increase the sensitivity to deeper chromophores.[4]

The coarse bundle used in this study has several advantages for clinical use. The size and number of the individual fiber cores enable construction of the system with entirely fiber optic connections. This architecture eliminates nearly all back reflections and provides greater efficiency in light delivery and collection, all of which improve the signal-to-background ratio (SBR) and acquisition speed. For comparison, the previous MDSFR system based on a pinhole and free-space optics was limited by poor SBR for the 0.2-mm effective fiber diameter, with SBR = 0.016 for the $\mu_s' = 3.6$ mm^{-1} phantom. Using all the-fiber-optic design presented here, the 0.2-mm effective diameter displayed SBR = 37 for the same phantom conditions, demonstrating an over 2000× improvement in SBR. In the current configuration, the fiber bundle system is able to complete a full measurement sequence capable of quantifying $\boldsymbol{\mu}_a$, $\boldsymbol{\mu}_s'$, $\boldsymbol{\gamma}$, and $\boldsymbol{Q}\mu_{a,x}^f$ of a localized volume of tissue in <8 s. With an overall bundle diameter slightly over 1.0 mm, the bundle used in this study is capable of being delivered to hollow organs through an endoscope or used as a simple handheld probe for superficial tissues and open surgical sites. Additionally, the maximum effective fiber diameter of 1.0 mm provides measurement depth sufficient for probing the superficial vasculature lying beneath epithelial tissue and the longer photon path length increases the sensitivity to low concentrations of tissue chromophores.

While the liquid optical phantoms used in this study are well suited for validation and characterization of the system, they represent an idealized tissue environment in which the optical properties are spatially homogeneous. The different fiber diameters used in MDSFR measure over different tissue depths, but assume consistent scattering properties in the simultaneous solution of Eq. (3). Because the MDSFR system guarantees colocalization of the effective fiber diameter, the spatially averaged scattering properties sampled by each fiber diameter are expected to be quite similar in most tissues. However, the effect of layered tissue with stratified optical properties on MDSFR measurements has yet to be investigated. Similarly, the quantitative fluorescence model assumes homogeneous distribution of fluorophores as well as scatterers, and could be potentially confounded by unequal distributions of one or the other. Given the limited measurement volumes,[4] any such heterogeneities are expected to be small; however, the effects of tissue optical property variations on the models will be the subject of future study.

5 Conclusion

We have demonstrated a robust MDSFR/SFF system capable of quantifying $\boldsymbol{\mu}_a$, $\boldsymbol{\mu}_s'$, $\boldsymbol{\gamma}$, and $\boldsymbol{Q}\mu_{a,x}^f$ from a small volume of tissue in one 8-s measurement, making it well suited for use in a clinical environment. The increased speed and robustness in comparison to the previous pinhole-based proof-of-concept system are a result of the elimination of free-space optics. While system calibration is critical to accurate optical property measurement, the daily calibration of the system requires only two simple measurements in liquid samples and an automated integrating sphere measurement, which are guided by the user interface for easy use by clinicians.

Using liquid optical phantoms, we have demonstrated that the system uses a fiber bundle to accurately simulate a variable-diameter solid-core fiber for both SFR and SFF spectroscopy. The effective path lengths and reflectances measured from the fiber bundle system match with those measured by the solid-core fibers and the extracted scattering properties $\boldsymbol{\mu}_s'$ and $\boldsymbol{\gamma}$ agree well with predicted values. Notably, we have used this system to demonstrate combined MDSFR/SFF spectroscopy, wherein the scattering and absorption properties are accurately quantified and then used to provide correction for quantitative fluorescence spectroscopy. Future work will investigate the use of this technique in stratified tissue optical properties and the integration of this system into clinical optical property measurements.

Acknowledgments

This research was supported by funding from the Center for Translational Molecular Medicine (CTMM).

References

1. I. J. Bigio and S. G. Bown, "Spectroscopic sensing of cancer and cancer therapy: current status of translational research," *Cancer Biol. Ther.* **3**(3), 259–267 (2004).
2. A. Wax and V. Backman, *Biomedical Applications of Light Scattering*, McGraw-Hill Professional Publishing, New York (2009).
3. J. R. Lakowicz, *Principles of Fluorescence Spectroscopy*, Springer London, Limited, London (2006).
4. S. C. Kanick et al., "Monte Carlo analysis of single fiber reflectance spectroscopy: photon path length and sampling depth," *Phys. Med. Biol.* **54**(22), 6991–7008 (2009).
5. S. C. Kanick, H. J. C. M. Sterenborg, and A. Amelink, "Empirical model of the photon path length for a single fiber reflectance spectroscopy device," *Opt. Express* **17**(2), 860–871 (2009).

6. S. C. Kanick et al., "Measurement of the reduced scattering coefficient of turbid media using single fiber reflectance spectroscopy: fiber diameter and phase function dependence," *Biomed. Opt. Express* **2**(6), 1687–1702 (2011).
7. T. J. Pfefer et al., "Temporally and spectrally resolved fluorescence spectroscopy for the detection of high grade dysplasia in Barrett's esophagus," *Lasers Surg. Med.* **32**(1), 10–16 (2003).
8. J. C. Finlay et al., "Interstitial fluorescence spectroscopy in the human prostate during motexafin lutetium-mediated photodynamic therapy," *Photochem. Photobiol.* **82**(5), 1270–1278 (2006).
9. S. C. Kanick et al., "Integration of single-fiber reflectance spectroscopy into ultrasound-guided endoscopic lung cancer staging of mediastinal lymph nodes," *J. Biomed. Opt.* **15**(1), 017004 (2010).
10. S. C. Kanick et al., "Characterization of mediastinal lymph node physiology in vivo by optical spectroscopy during endoscopic ultrasound-guided fine needle aspiration," *J. Thorac. Oncol.* **5**(7), 981–987 (2010).
11. S. C. Kanick et al., "Method to quantitate absorption coefficients from single fiber reflectance spectra without knowledge of the scattering properties," *Opt. Lett.* **36**(15), 2791–2793 (2011).
12. U. A. Gamm et al., "Measurement of tissue scattering properties using multi-diameter single fiber reflectance spectroscopy: in silico sensitivity analysis," *Biomed. Opt. Express* **2**(11), 3150–3166 (2011).
13. U. A. Gamm et al., "Quantification of the reduced scattering coefficient and phase-function-dependent parameter γ of turbid media using multi-diameter single fiber reflectance spectroscopy: experimental validation," *Opt. Lett.* **37**(11), 1838–1840 (2012).
14. A. Ishimaru, *Wave Propagation and Scattering in Random Media*, Academic Press, New York (1978).
15. V. Turzhitsky et al., "A predictive model of backscattering at subdiffusion length scales," *Biomed. Opt. Express* **1**(3), 1034–1046 (2010).
16. S. C. Kanick et al., "Method to quantitatively estimate wavelength-dependent scattering properties from multidiameter single fiber reflectance spectra measured in a turbid medium," *Opt. Lett.* **36**(15), 2997–2999 (2011).
17. F. van Leeuwen-van Zaane et al., "In vivo quantification of the scattering properties of tissue using multi-diameter single fiber reflectance spectroscopy," *Biomed. Opt. Express* **4**(5), 696–708 (2013).
18. S. C. Kanick et al., "Semi-empirical model of the effect of scattering on single fiber fluorescence intensity measured on a turbid medium," *Biomed. Opt. Express* **3**(1), 137–152 (2012).
19. C. L. Hoy et al., "Use of a coherent fiber bundle for multi-diameter single fiber reflectance spectroscopy," *Biomed. Opt. Express* **3**(10), 2452–2464 (2012).
20. P. R. Bargo, S. A. Prahl, and S. L. Jacques, "Collection efficiency of a single optical fiber in turbid media," *Appl. Opt.* **42**(16), 3187–3197 (2003).
21. S. C. Kanick et al., "Extraction of intrinsic fluorescence from single fiber fluorescence measurements on a turbid medium," *Opt. Lett.* **37**(5), 948–950 (2012).
22. R. Michels, F. Foschum, and A. Kienle, "Optical properties of fat emulsions," *Opt. Express* **16**(8), 5907–5925 (2008).
23. F. Bevilacqua and C. Depeursinge, "Monte Carlo study of diffuse reflectance at source-detector separations close to one transport mean free path," *J. Opt. Soc. Am. A* **16**(12), 2935–2945 (1999).
24. R. Sjöback, J. Nygren, and M. Kubista, "Absorption and fluorescence properties of fluorescein," *Spectrochim. Acta, Part A* **51**(6), L7–L21 (1995).
25. P. D. Ninni, F. Martelli, and G. Zaccanti, "Intralipid: towards a diffusive reference standard for optical tissue phantoms," *Phys. Med. Biol.* **56**(2), N21–N28 (2011).